

6.0 BALLOON-BORNE VERTICAL PROFILES OF OZONE, METHANE, NON-METHANE HYDROCARBONS, NITROGEN OXIDES AND METEOROLOGICAL PARAMETERS

Detlev Helmig, Chelsea Stephens, Jeong-Hoo Park, Jacques Hueber, Patrick Boylan, Jason Evans

Institute of Arctic and Alpine Research, University of Colorado Boulder

6.1 Objective

The primary objective of this project was to investigate the vertical distribution of relevant trace gases, including ozone, methane, non-methane hydrocarbons, and nitrogen oxides, and meteorological parameters to understand the vertical structure of ozone precursors and ozone production with linkages to boundary-layer conditions during and between inversion events. This project utilized measurements from a surface tower, the CU-INSTAAR tethered balloon platform for measurements of vertical profiles of trace gases, and a NOAA-GMD tethered sonde platform for measurement of ozone and meteorological parameters.

6.2 Experimental Methods and Instrumentation

6.2.1 Study Site and Duration

The study by CU-INSTAAR was conducted at the Horsepool site (~1569 m a.s.l) in the Uinta Basin from January 25 through February 19, 2013. Between two to four CU researchers were on-site at all times throughout this period to allow for 24/7 operation, including midnight tethered sonde launches.

6.2.2 Experimental Set-Up

Vertical profiles were conducted using a 2 m flux tower, a tethered SkyDoc balloon, and tethered electrochemical cell (ECC) ozone and radio sondes. A trailer housing the instruments was located approximately 10 m from the tower and balloon launch sites. A schematic of the experimental set-up is shown in Figure 6-1.

Vertical profiles of trace gases were conducted at five sampling heights. Sampling lines were placed approximately 30 cm into the snowpack, at 2 m on the flux tower, and at three heights on the SkyDoc balloon tether line, nominally at 50 m, 100 m, and 150 m (balloon heights fluctuated with time). The SkyDoc flew at a maximum height of 500 ft (~170 m) and was raised and lowered using a hydraulic winch. Data coverage with the SkyDoc was nearly continuous, with only brief periods when the balloon was taken down due to inclement weather (e.g., high winds, icing conditions) or for inter-comparisons and instrument calibrations.

Sampling lines were made of PFA Teflon. Balloon sampling lines were approximately 650 ft in length and colored black to prevent in-line photochemistry. These sampling lines have been previously shown to have excellent performance for sampling both ozone and hydrocarbons with very little line loss (< 5 % for ozone and 3 % for hydrocarbons). Sampling lines were

plumbed into a sampling manifold to which the analytical instruments were connected. Four of the sampling lines were continuously measured for ozone using dedicated ozone monitors. All other species were sampled through a switching valve that switched between the five inlets (including the snow inlet) every six minutes, such that a full vertical profile was conducted every 30 minutes.

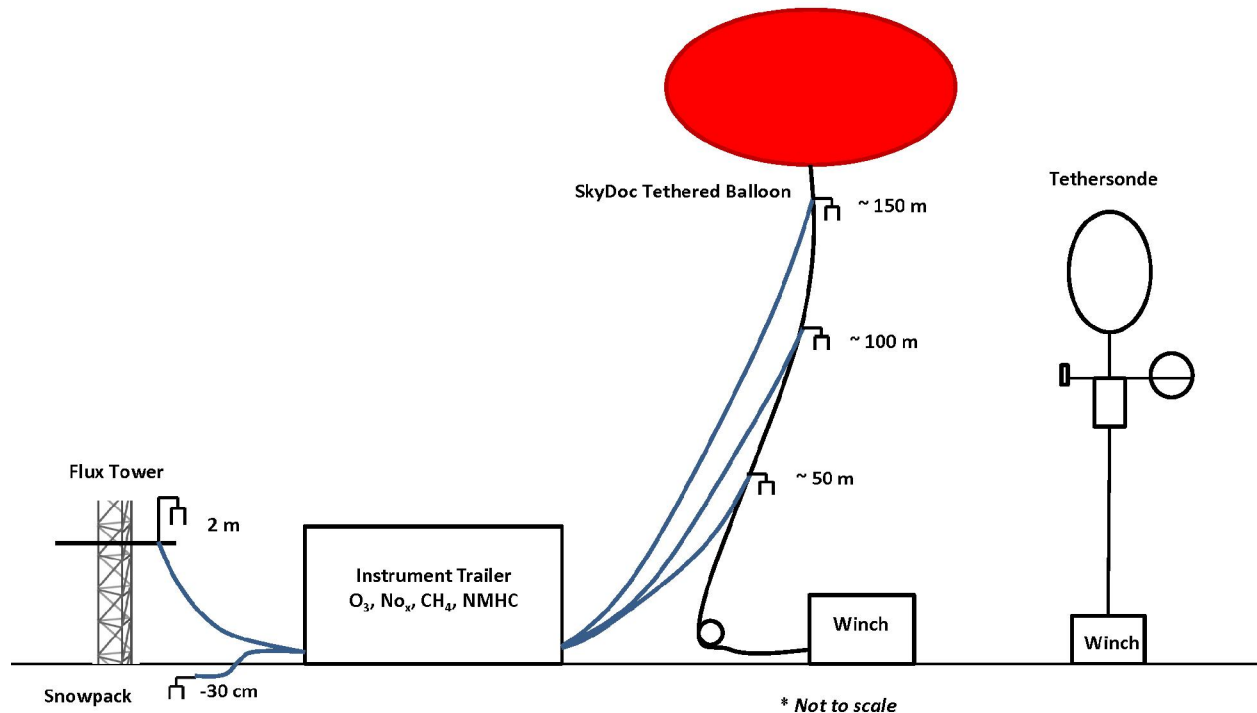


Figure 6-1. Schematic of the CU-INSTAAR experimental setup during UBOS 2013.

Vertical profiles of ozone and meteorological parameters to a height of approximately 500 m above ground level were conducted using ECC and radio tethersondes provided by NOAA-GMD. In addition, a battery-powered Kestrel sonde measured temperature, humidity, wind speed and wind direction. Meteorological parameters (temperature, pressure, wind speed, wind direction) were also measured on the 2 m flux tower. Sondes were raised and lowered using a small electric winch. Five to six sonde launches were conducted per day, including an early morning launch (approximately 6:00) and a midnight launch. Figure 6-2 shows the record of sonde launches illustrating the excellent data coverage achieved.

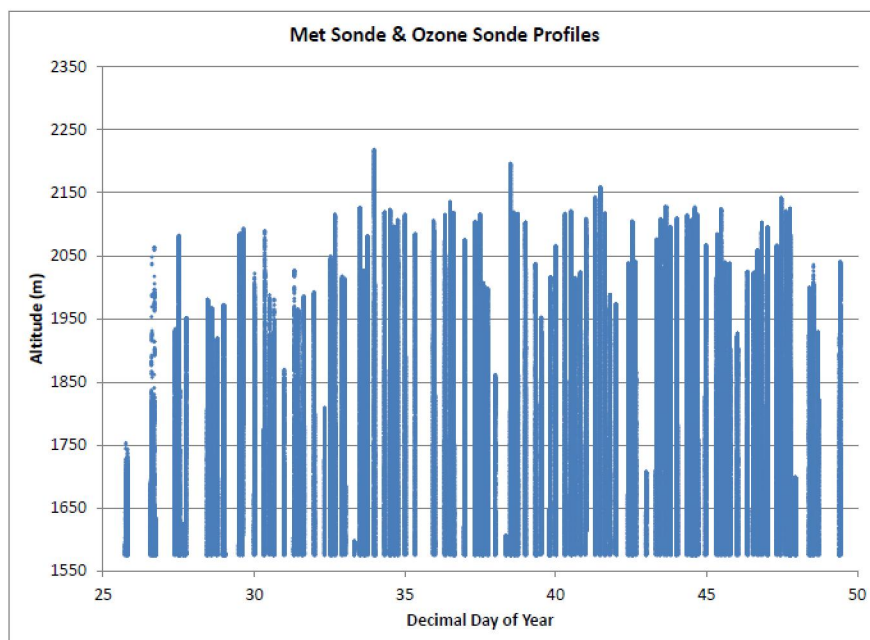


Figure 6-2. Record of ECC sonde launches and balloon height.

6.2.3 Instrumentation and Procedures

Ozone was measured continuously from the 2 m tower and the three balloon lines using four dedicated commercial UV-absorbance ozone monitors (Thermo, API, and Monitor Labs). An additional Thermo 49i ozone monitor was placed on the switching manifold, measuring ozone at each of the five heights (including in snow) for six minutes each. All ozone monitors were calibrated using a NOAA-GMD referenced laboratory standard prior to deployment. The monitors were routinely zeroed on site using an ozone scrubber, and inter-comparisons were conducted when all of the sampling inlets were placed side-by-side on the 2 m tower.

Methane was measured using a Baseline Series 8900 gas chromatograph with flame-ionization detection loaned to CU-INSTAAR by the State of Utah Department of Environmental Quality. The instrument continuously monitored methane with a time resolution of three minutes using a packed column for separation. Automated calibrations were performed twice a day using a gas standard provided with the instrument. The methane GC was connected to the switching valve on the sampling manifold for vertical profiles.

Nitrogen oxides (NO and NO_x + NO_y) were measured using a commercial Teledyne NO_x monitor with a molybdenum oxide converter also loaned to CU-INSTAAR by State of Utah Department of Environmental Quality. The instrument continuously monitored NO and NO_x (with the reported NO_x also including a fraction of NO_y due to the limited NO_x selectivity of the converter) at one-minute time resolution and was connected to the switching valve on the sampling manifold for vertical profiles.

Non-methane hydrocarbons (NMHC) were measured using a field-portable gas chromatograph with flame ionization detection. The GC is a fully automated instrument optimized for analysis of C2-C10 NMHC, covering saturated and unsaturated NMHC and aromatic compounds to the xylenes. The instrument operates by preconcentrating NMHC from 0.5 L of sampled air on a Peltier-cooled micro-absorbent trap. The trap is then flash-heated and NMHC are separated on an Al₂O₃ KCl PLOT column by temperature-programmed chromatography followed by flame-ionization detection. This instrument had two identical sampling channels such that one channel continuously sampled from the 2 m tower inlet, and the second channel was placed on the switching valve to conduct vertical profile measurements. The measurement time resolution of the NMHC GC was 36 minutes. Automated calibrations were performed daily from a certified VOC standard gas cylinder. Additional calibration standards and instrument zeroes were performed just prior and to the end of the campaign.

In addition to the in-situ GC measurements, volatile organic compounds (VOC) were also analyzed from whole air samples collected using a Portable Flask Package (PFP) and Portable Compressor Package (PCP). The PFP contains twelve 0.75 L glass flasks that are opened and filled sequentially to 40 psi via computer control. A total of 90 whole air samples were collected during the campaign distributed among the five inlets. The PFPs were analyzed for VOC at the CU-INSTAAR laboratory in Boulder by GC-FID/mass spectrometry detection. The laboratory GC operates on the same principles as the field GC described above. Instrument blanks and VOC standards are analyzed before and after each set of 12 flask samples. Our laboratory is the core of the Global VOC Monitoring Network program and our standard scale has been cross-referenced on multiple occasions against other participating international laboratories. Our laboratory was audited by the World Calibration Center for VOC twice and found to meet all quality criteria set by the WMO GAW program for VOC.

Meteorological instrumentation was installed on the 2 m tower. This consisted of a wind vane and cup anemometer for wind speed and direction, an RTD temperature probe with aspirated shield, and upward and downward looking radiation sensors.

The tethered instrumentation was loaned to CU-INSTAAR by NOAA-GMD. Briefly, these sondes consisted of an ECC ozone sonde that has been used extensively for quantifying ozone, and a radiosonde that measures altitude, temperature, pressure, and water vapor.

6.3 Results

6.3.1 Ozone

The 2013 campaign experienced several periods of high ozone build-up periods during sustained inversion events. In contrast to the 2012 study, during which there was no snow and ozone remained in the range of 10 – 60 ppbv, in 2013 there was persistent snow-cover throughout the campaign and ozone reached as high as 150 ppbv (Fig. 6-3).

There were three distinct ozone build-up events during the time that the CU-INSTAAR instruments were at Horsepool. Upon arrival at the site, we captured the tail-end of the first event (Event 1) that lasted until January 26 and then was cleaned out by the passage of a low-pressure system. Event 2 began January 31 with ozone increasing until February 7. This was again cleaned out by the passage of a low-pressure system. Event 3 began February 13 and lasted until February 18 when there was a partial cleaning out of the basin. In 2012, although there were no high ozone build-up events, ozone did show a very dynamic behavior with a diurnal profile that peaked in the afternoon and a daytime/nighttime amplitude of 30 – 40 ppbv. The 2013 ozone record shows this same diurnal behavior superimposed on the build-up events with an amplitude of 20 – 50 ppbv.

The vertical distribution of ozone throughout the duration of the campaign is illustrated in Figure 6-4 as a color contour plot showing the full record of the ECC sonde ozone data for Horsepool. The three high ozone build-up events are evident in the warmer colors on the color scale, which here goes to 175 ppbv. The vertical structure reveals that ozone builds up in both mole fraction and in height during the inversion events. The highest ozone is consistently confined within the lowest 100 – 150 m above ground level and at many times appears to be well-mixed within the shallow boundary layer. With the exception of one day, throughout the campaign relatively low ozone (i.e., < 75 ppbv) is present above 1900 m a.s.l. The cleaning out periods (i.e., January 28 – 31 and February 10 – 11) brought relatively clean background air down the surface, resulting in ground-level ozone values on the order of 30 – 60 ppbv.

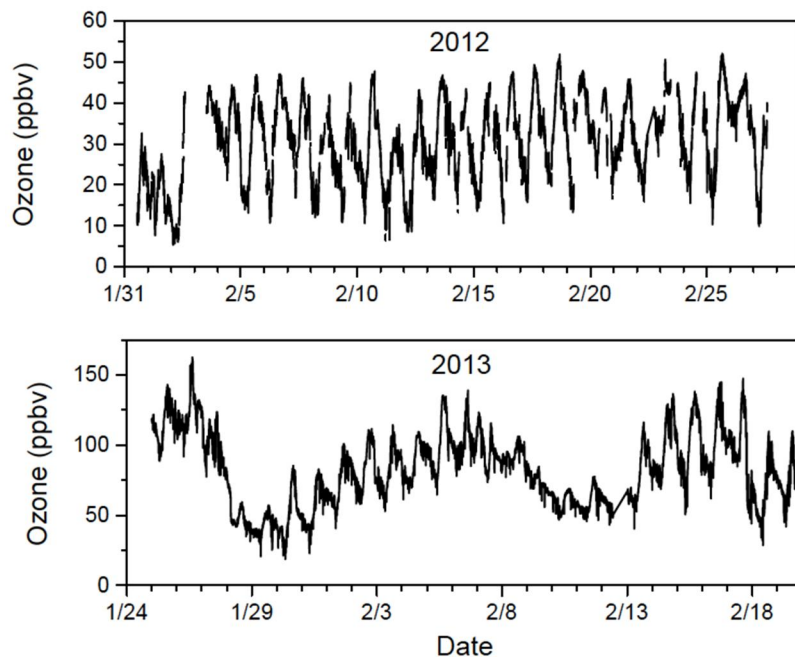


Figure 6-3. Comparison of ozone measured at 2 m height from the 2012 and 2013 UBOS campaigns (note different y-axis scales).

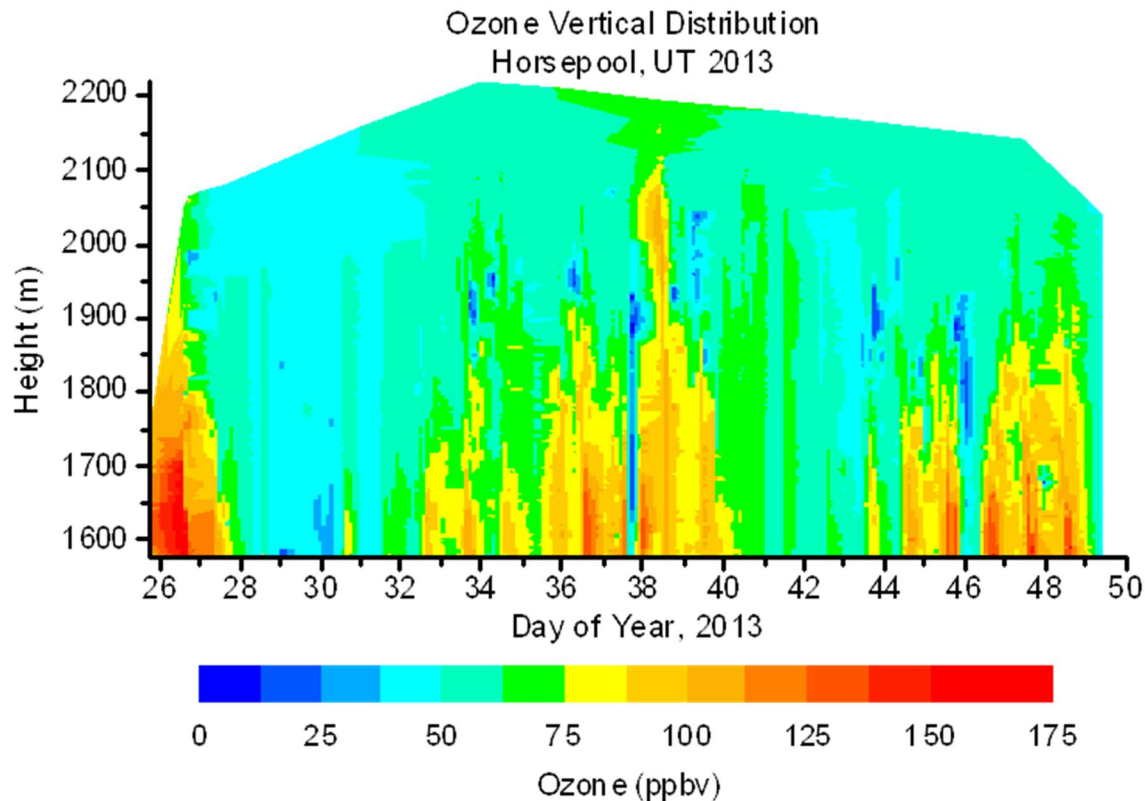


Figure 6-4. Contour plot showing the complete record of ozone measurements acquired from the ECC tether sondes launched by the CU-INSTAAR group at Horsepool.

A closer examination of individual ozone vertical profiles reveals the shallow, near-surface enhancement of photochemical ozone production. Figure 6-5 shows ECC sonde profiles for four days of the campaign, contrasting a relatively low ozone period (January 30 and 31) with an ozone build-up period (February 12 and 13). Here it can be seen that for both periods the ozone profiles are relatively consistent with height during the midnight and/or early morning profiles, but that during the day there is photochemical ozone production that is almost entirely confined to the lowest 100 – 150 m above ground level. Even on days prior to the beginning of an ozone build-up event (i.e., January 30) there is significant daytime ozone production near the surface. Notably, the ozone profiles throughout the day tend to converge to a common value in the highest ~ 200 m, or roughly above 1850 m a.s.l., indicating the presence of background air and that the sonde had reached beyond the top of the inversion layer.

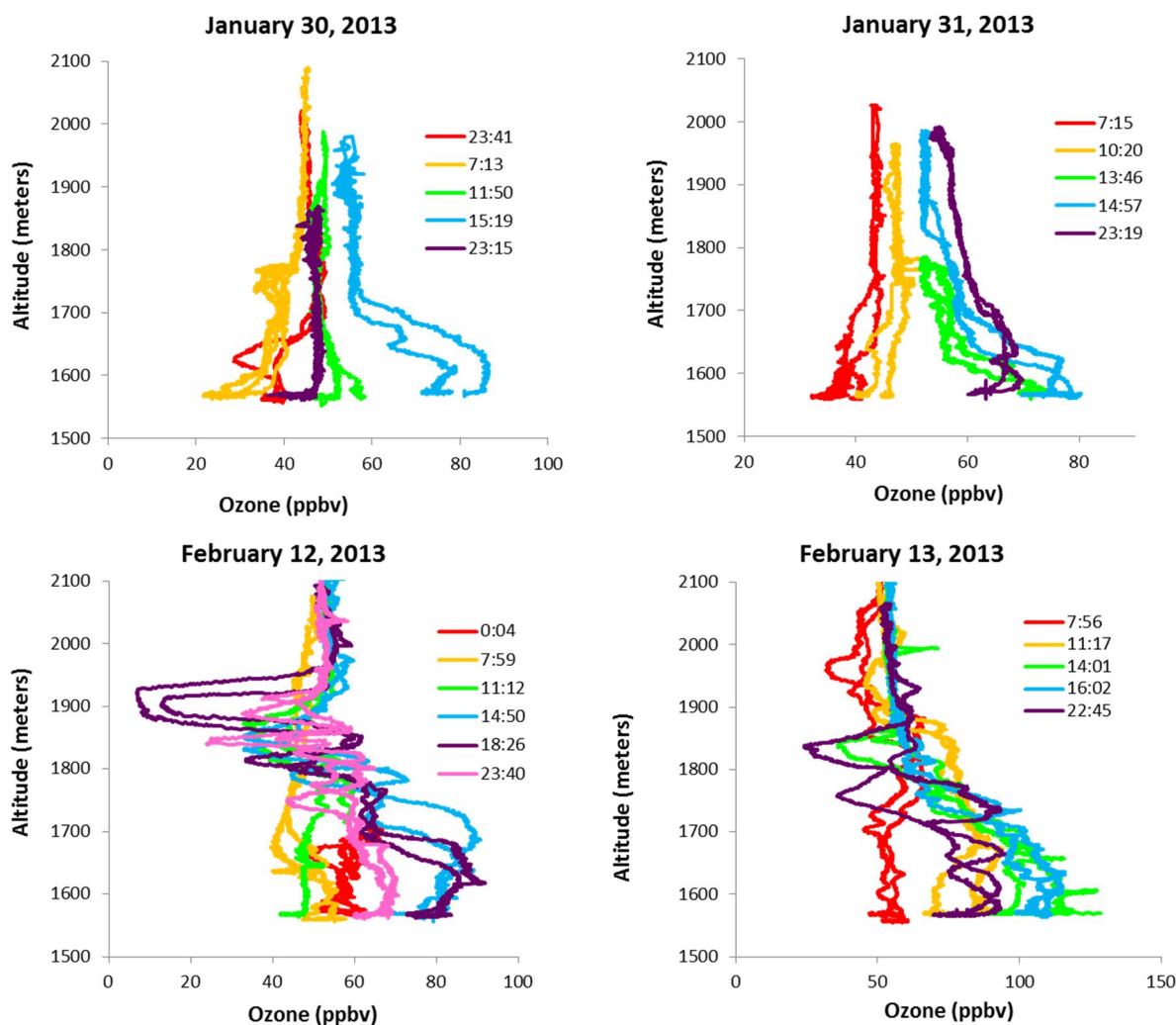


Figure 6-5. Ozone vertical profiles from the ECC tethersonde for four days of the campaign, illustrating an unstable, relatively low ozone period (January 30 and 31) and a high ozone period during an inversion event (February 12 and 13) (please note the different x-axis scales of the graphs).

6.3.2 Methane

As with ozone, methane values were significantly enhanced during the 2013 campaign as compared to 2012, although both years had methane values that were highly elevated over the regional background (~1.9 ppmv). Whereas in 2012 methane had the highest excursions up to ~10 ppmv, in 2013 methane was often above 15 ppmv at the surface. Figure 6-6 compares the methane time series from 2 m for the 2012 and 2013 campaigns (purple trace) overlaid on ozone (black trace). Most noticeable in comparison of these two data series is the clear build-up in methane mole fraction observed in 2013 coincident with the ozone build-up periods. Indeed, the ozone:methane correlation plots in Figure 6-7 reveal the positive correlation between these two species in 2013, a feature that was absent in 2012. The sharp and short-

lived excursions of methane up to and above 20 $\mu\text{mol/mol}$ indicate an influence from nearby point-sources of methane in the region.

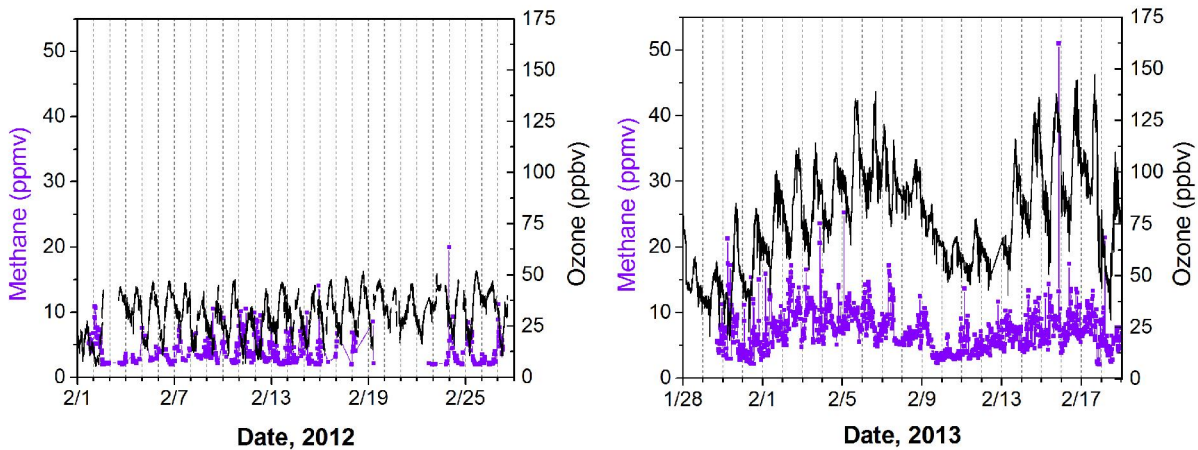


Figure 6-6. Time series of methane (purple) and ozone (black) comparing the 2012 and 2013 campaigns.

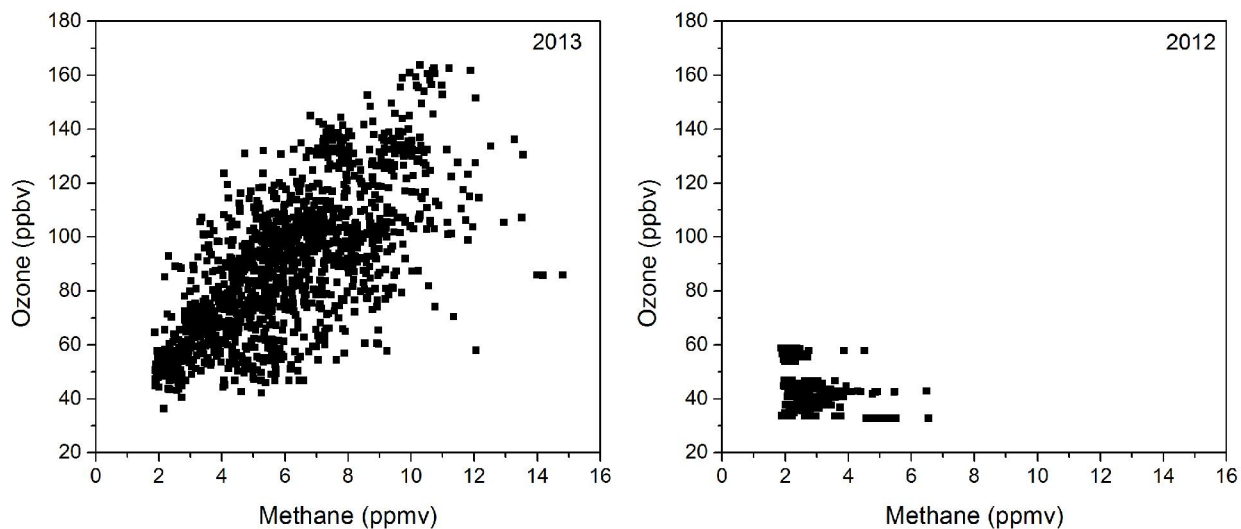


Figure 6-7. Correlations of ozone and methane for 2013 (left) and 2012 (right).

The average diurnal behavior of methane also showed marked differences between 2012 and 2013 (Figure 6-8A), which is of interest for this relatively long-lived compound. In 2012, methane showed a diurnal pattern with highest values in the early morning hours, consistent with overnight buildup in a relatively stable nocturnal surface layer, followed by a mid-afternoon minimum with little variability, consistent with relatively deep vertical mixing induced by upward surface heat flux from the bare ground. In 2013, on the other hand,

methane peaked at 08:00 MST and had a less distinct minimum during the afternoon hours, consistent with a much more stable afternoon surface layer over the snow covered ground.

The vertical distribution of methane as measured from the SkyDoc tethered balloon is shown in Figure 6-8B. These data reveal that the highest average mole fraction of methane was present nearest the surface and that the surface level methane showed the highest variability.

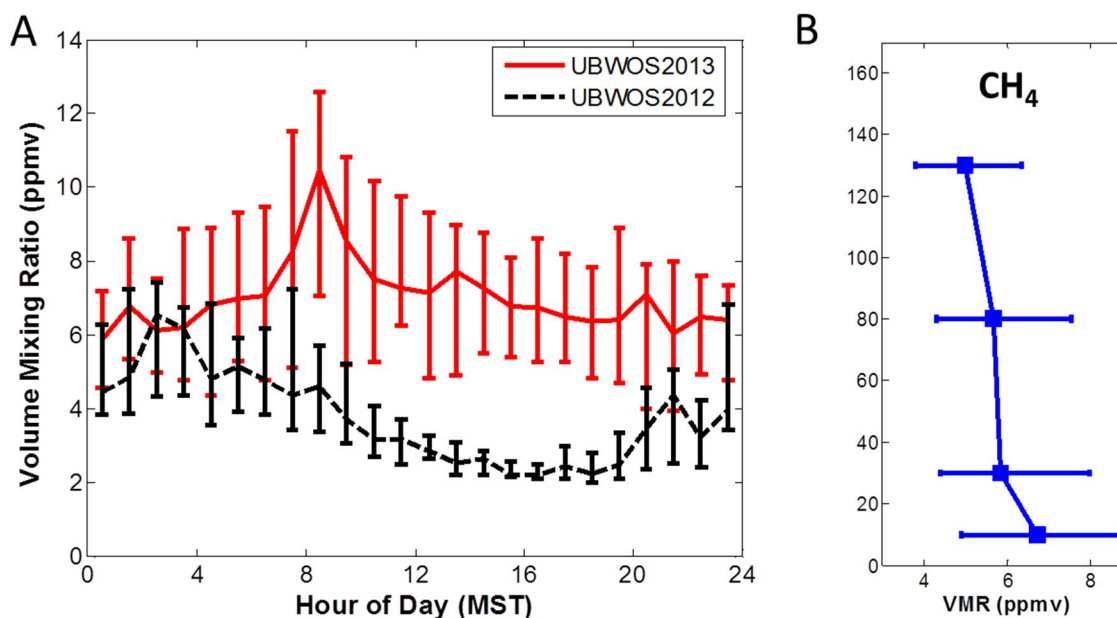


Figure 6-8. Panel A: Diurnal average for methane comparing the 2012 (black) and 2013 (red) campaigns. Panel B: Average (plus or minus one standard deviation) methane vertical distribution for the 2013 campaign.

6.3.3 Nitrogen Oxides

NO_x levels showed a high variability, with most values ranging between 5-20 ppbv, and occasional spikes exceeding 50 ppbv (Fig. 6-9). Overall NO_x was about 2-3 times higher in 2013 compared to 2012. The comparison of the composite diurnal cycles (Fig. 6-10) illustrates that the enhancement was particularly pronounced during mid-day to afternoon hours. This NO_x comparison points to a similar conclusion as for methane and NMHC (below) that primary emissions accumulated to higher levels in 2013 due to reduced ventilation of the surface layer. The high variability in NO_x may also point towards a relatively inhomogeneous distribution of NO_x sources. NO remained below 0.1 ppbv at night, but rose sharply during morning hours to reach average levels of ~ 2 ppbv around noon time (Fig. 6-9). NO was $\sim 50\%$ higher in 2013 compared to 2012. The tethered balloon vertical profile measurements (Fig. 6-11) showed highest NO_x mole fractions at the surface and decreasing levels with height, indicating that most of the NO_x results from nearby sources.

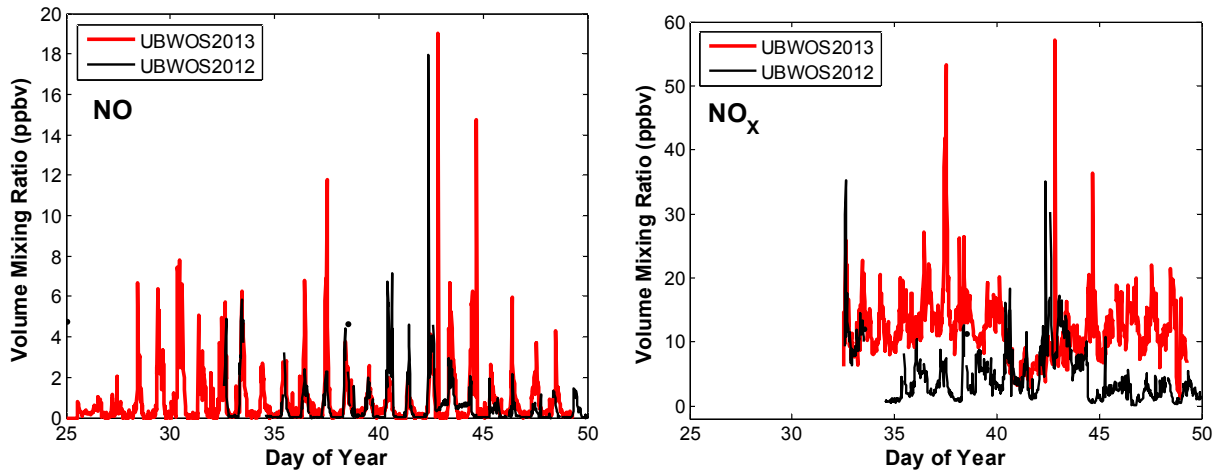


Figure 6-9. Time series of NO and NO_x from the 2 m tower comparing the 2012 (black) and 2013 (red) campaigns.

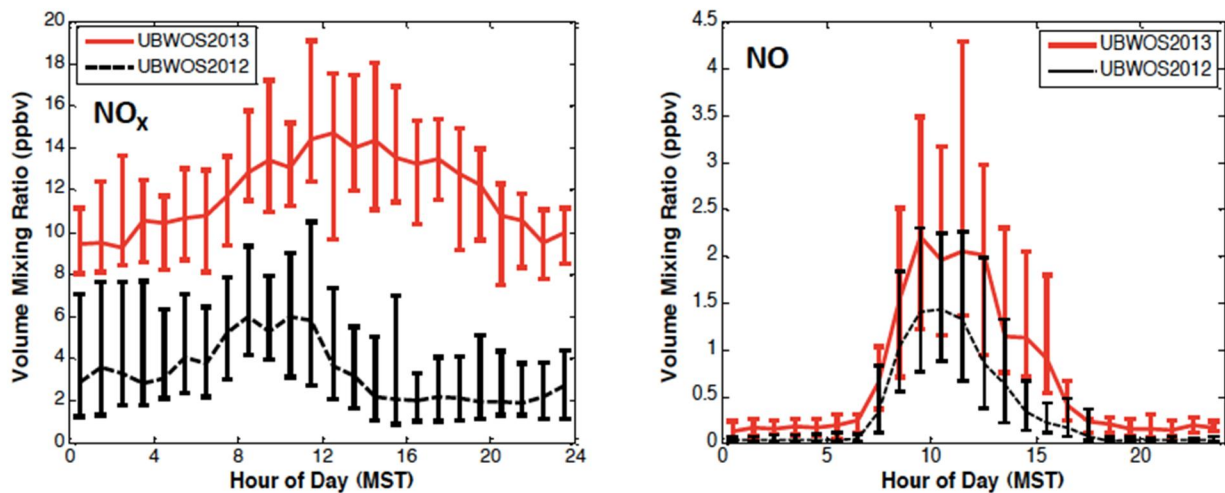


Figure 6-10. Diurnal averages of NO_x and NO from the 2 m tower comparing the 2012 (black) and 2013 (red) campaigns.

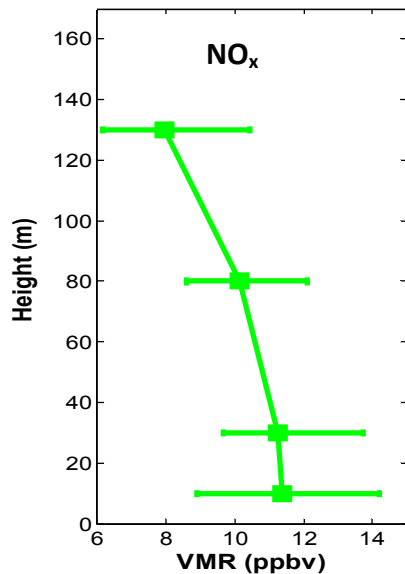


Figure 6-11. Mean vertical distribution plus standard deviation of NO_x during the 2013 campaign.

6.3.4 Non-Methane Hydrocarbons

Non-methane hydrocarbons serve as precursors to photochemical ozone formation. Data from 2012 and 2013 both show that the light alkanes (i.e., C₂ – C₅) dominate the NMHC composition in the Uinta Basin. The mass fraction of an individual NMHC compound generally decreased with increasing molecule size. As discussed with other species, the mole fraction of NMHC was significantly enhanced in 2013 in comparison to 2012. Figure 6-12 demonstrates this by showing ethane (red) and propane (blue) overlaid on ozone (black). As with methane, these alkanes show a similar temporal behavior as ozone, building up during the inversion periods and then cleaning out to lower levels (e.g., <100 ppbv for ethane) when a low-pressure system would bring in air from the west.

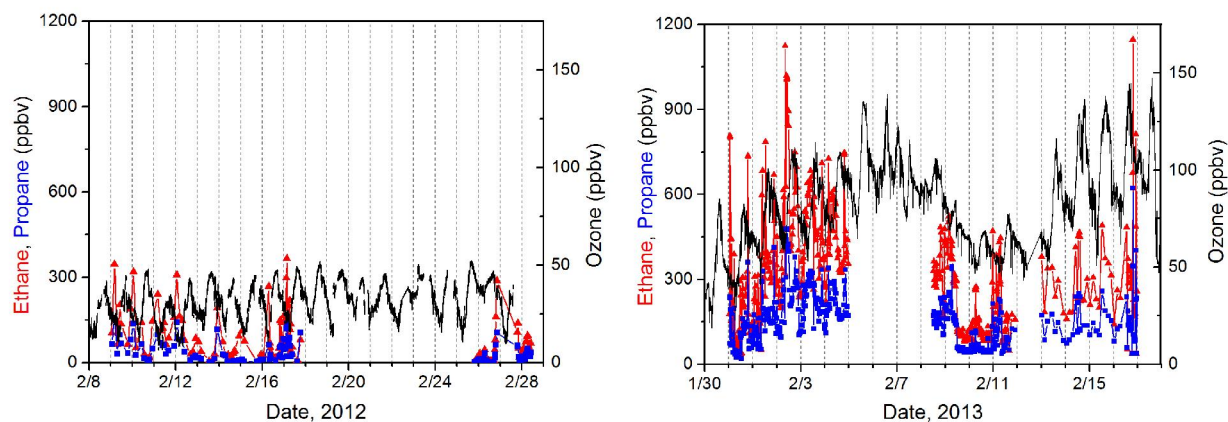


Figure 6-12. Ethane (red) and propane (blue) time series from the 2 m tower overlaid with ozone (black) comparing the 2012 and 2013 campaigns.

The NMHC mole fractions observed in the Uinta Basin in both 2012 and 2013 greatly exceeded the regional background values for 40°N as determined by the NOAA-INSTAAR Global Flask Network. The average ethane value for 2013, 320 ppbv, exceeded background by a factor of 160. However, the maximum ethane observed in 2013, which was greater than 1100 ppbv, corresponded to an enhancement of 550-fold over the regional background. The longer alkanes, propane through pentane, had an even greater enhancement over background values than did ethane (Table 6-1).

Table 6-1. Average values for C2-C5 alkanes observed in 2012 and 2013 in comparison to regional background for 40°N in February as determined by the NOAA-INSTAAR Global Flask Network.

Compound	Uinta 2012 Average (ppbv)	Uinta 2013 Average (ppbv)	Global Background 40°N, February (ppbv)	Enhancement Factor: Uinta 2013 vs. Background
Ethane	73	320	2.0	160
Propane	32	160	0.64	250
<i>i</i> -Butane	6.7	33	0.09	367
<i>n</i> -Butane	12	51	0.17	300
<i>i</i> -Pentane	5.4	22	0.06	367
<i>n</i> -Pentane	5.0	20	0.04	500

As with the alkanes, the simple aromatic compounds (e.g., benzene, toluene) exhibited strong enhancements in the Uinta Basin, and experienced build-up concurrent with the ozone events. Figure 6- 13 illustrates this with benzene (orange) and toluene (purple) overlaid with ozone (black). Both benzene and toluene were consistently greater than 1 ppbv and at times reached over 10 ppbv. The tight correlation between benzene and ethane indicates a common source for both of these compounds.

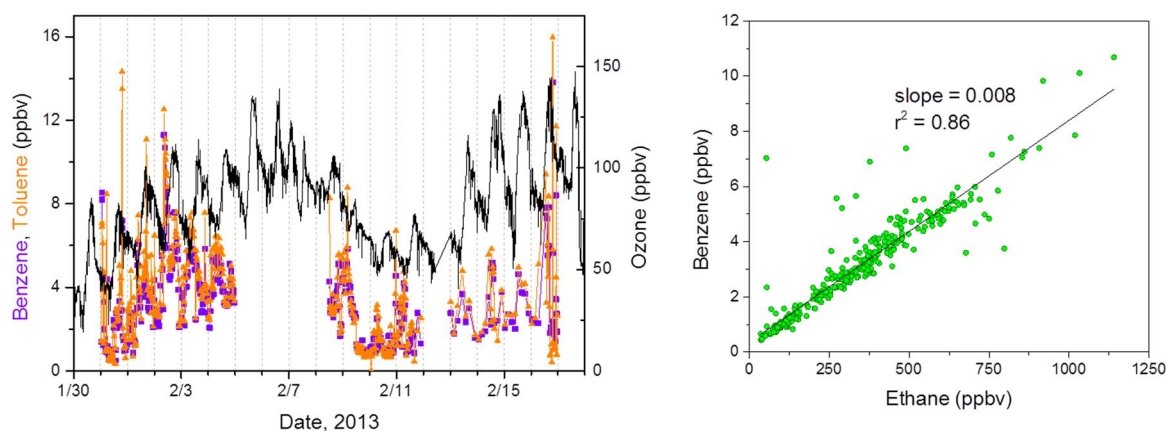


Figure 6-13. Left: Time series of benzene (orange) and toluene (purple) overlaid with ozone (black) for the 2013 campaign. Right: Linear correlation of benzene and ethane for 2013.

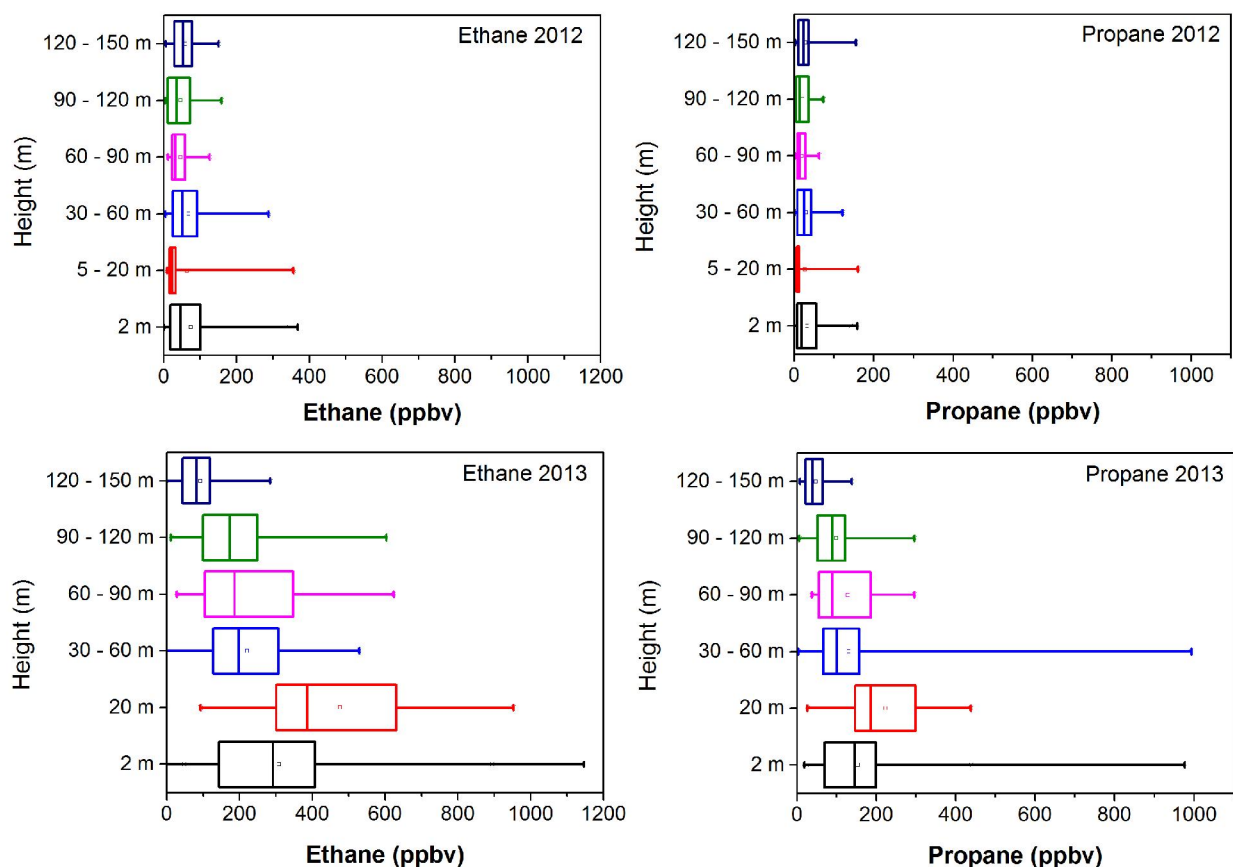


Figure 6-14. Statistics of the vertical distributions of ethane and propane comparing the 2012 (top) and 2013 (bottom) campaigns. Here, the square marker represents the mean value, the edges of the box represent the 25th and 75th percentiles, the line in the box represents the median value, and the “whiskers” represent the minimum and maximum values.

Significant differences were observed in the vertical distribution of the NMHC between the 2012 and 2013 campaigns. Figure 6-14 shows the statistics of the vertical distribution of ethane and propane as box and whisker plots. These plots show the dramatic difference in mole fraction at the lowest heights, with the greatest values observed near the surface in 2013. The NMHC appear to be primarily enhanced in the lowest 100 m during the inversion conditions in 2013, consistent with the vertical ozone profiles observed. In 2012, stronger vertical mixing resulted in relatively consistent mole fractions throughout the column. Mole fractions of both compounds were, however, similar in 2012 and 2013 at the highest measurement levels.

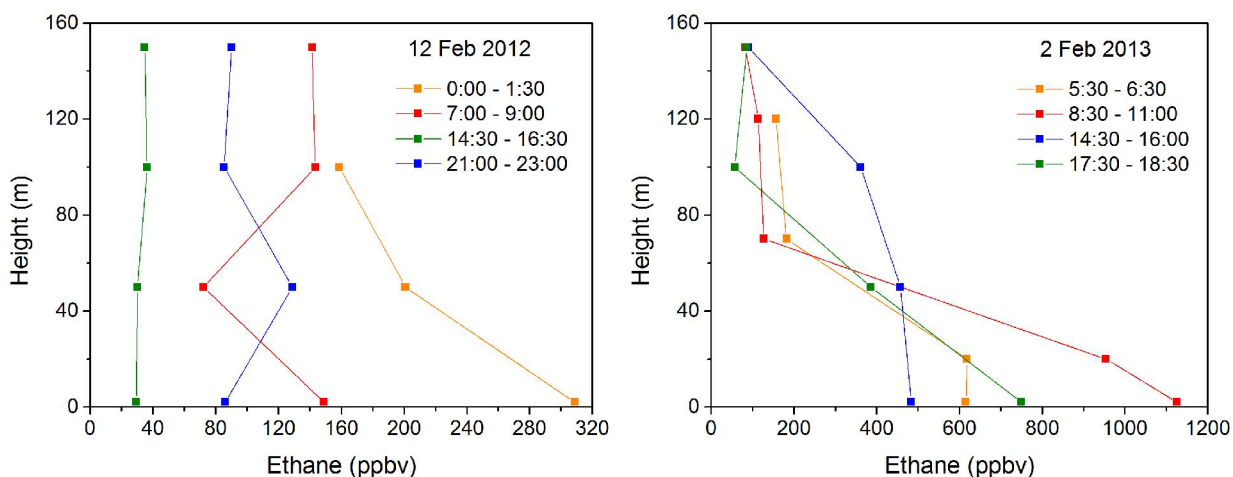


Figure 6-15. Examples of two days of ethane vertical profiles contrasting a day with relatively strong vertical mixing (February 12) with a day with a shallow boundary layer and minimal vertical mixing (February 2).

Individual vertical profiles of the NMHC (here shown for ethane in Figure 6-15) reveal the surficial nature of the strongest NMHC enhancements. Unlike for ozone, where mole fractions would build up during the day and reach an afternoon maximum due to photochemical production, ethane as a primary emission exhibited a more “plume-like” behavior with pockets of high NMHC passing over the measurement site in a more sporadic fashion.

6.3.5 Snowpack Air Ozone and NMHC Measurements

Ozone and NMHC were measured throughout the 2013 campaign through an inlet placed ~30 cm into the snowpack to sample snowpack air. The ozone record is shown in Figure 6-16A. Ozone within the snowpack air followed a nearly identical temporal pattern as ambient (2 m) ozone, but at significantly lower values. Snowpack ozone was attenuated by 50 – 80%, indicating that the snowpack is not a direct source of the high ozone in the Basin. This furthermore suggests chemical destruction and/or physical adsorption of ozone occurring in the snowpack. This destruction of ozone in the snowpack air is consistent with observations from Arctic and a Rocky Mountain high elevation site (Albert et al., 2002; Helmig et al., 2007; Peterson and Honrath, 2001; Bocquet and Helmig, 2007).

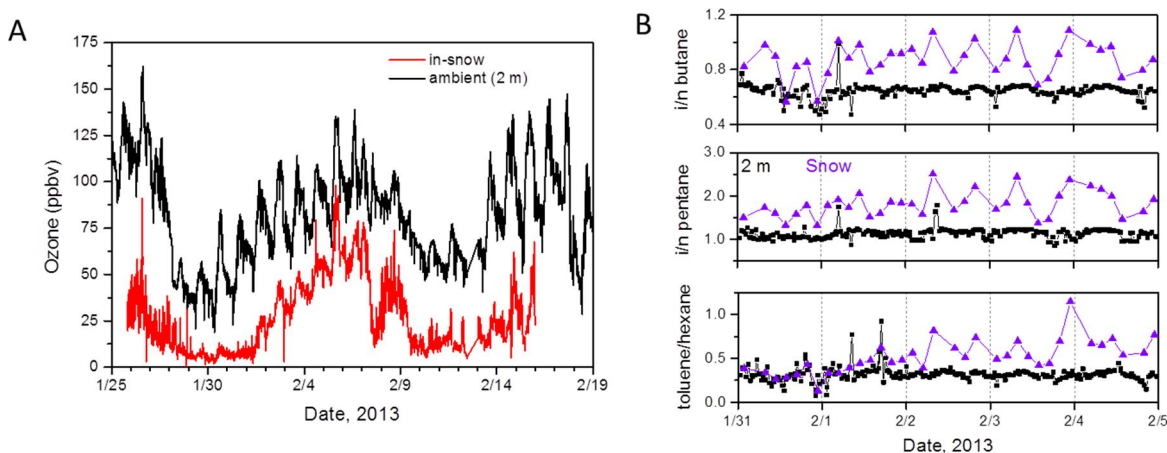


Figure 6-16. Panel A: Time series of ozone measured from the 2 m tower (black) and from the snowpack inlet (red). Panel B: Time series of select NMHC ratios from the 2 m tower (black) and from the snowpack inlet (purple).

Figure 6-16B shows time-series of select ratios of NMHC pairs determined from ambient measurements at the 2 m tower and from the snowpack air measurements with the snowpack inlet. Shown are the iso-butane:n-butane ratio, the iso-pentane:n-pentane ratio, and the toluene:hexane ratio. In each case, the ratios are enhanced in the snowpack relative to the ambient air. This enhancement indicates a preferential destruction of n-butane, n-pentane, and hexane relative to iso-butane, iso-pentane, and toluene, respectively. These ratios are indicators of active radical chemistry (Ariya et al., 1998; Jobson et al., 1994; Pszenny et al., 2007; Rudolph et al., 1997), and are suggestive of potential chlorine chemistry in the snowpack.

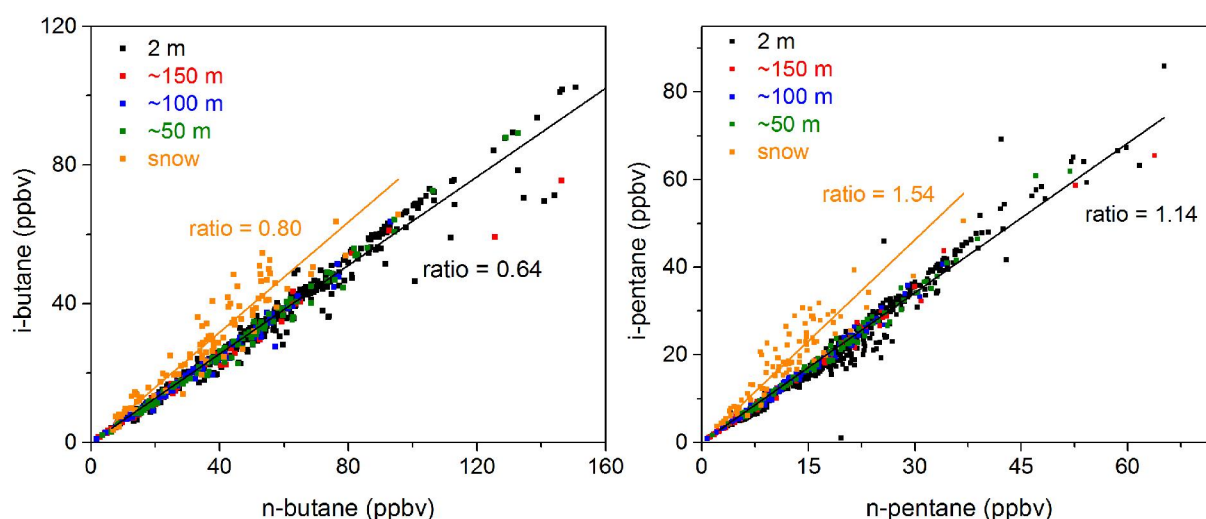


Figure 6-17. Correlation plots for iso-butane:n-butane and iso-pentane:n-pentane broken up by inlet height.

The iso-butane/n-butane and iso-pentane/n-pentane ratios have been used extensively in atmospheric research as a proxy for chlorine radical reactions, notably in Arctic environments, since direct measurements of halogen atoms have not been possible (Ariya et al., 1998; Boudries and Bottenheim, 2000; Jobson et al., 1994; Rudolph et al., 1997; Rudolph et al., 1999). This technique is based upon the differences in kinetic rate constants for Cl and OH radicals with these species. The OH radical reacts with both isomers of butane with approximately the same rate constant, and the same is true for the isomers of pentane. However, Cl atoms react preferentially (by a factor of ~ 1.5) with the n isomer of these compounds. Thus, an enhancement in these isomer ratios is suggestive, but not proof, of active chlorine radical chemistry. Figure 6-17 plots these two ratios, dividing the measurements by inlet height. Here it can be seen that all of the ambient data, regardless of height, clusters tightly around the 0.64 line for the butanes and the 1.14 line for the pentanes. The only data that do not lie on this line are the snowpack data, shown in orange. In both cases, the snowpack ratios are enhanced relative to the ambient air. Figure 6-18 illustrates this in another fashion, but plotting the iso-pentane:n-pentane ratio versus n-pentane and the iso-butane:n-butane ratio versus n-butane. When expressed in this manner, data that fall along a horizontal line would be indicative of OH-dominated oxidation chemistry, whereas data that fall along a vertical line would be indicative of Cl-dominated oxidation chemistry (Jobson et al., 1994). Here it can be seen that, again, the snowpack data deviate significantly from all ambient data, suggesting active radical chemistry occurring in the snowpack air. It should also be noted that ethane, the least reactive of these NMHC, exhibits a nearly identical values between snowpack and 2 m measurements, indicating that the differences in NMHC observed here are not merely a result of slower transport (via diffusion) through the snowpack.

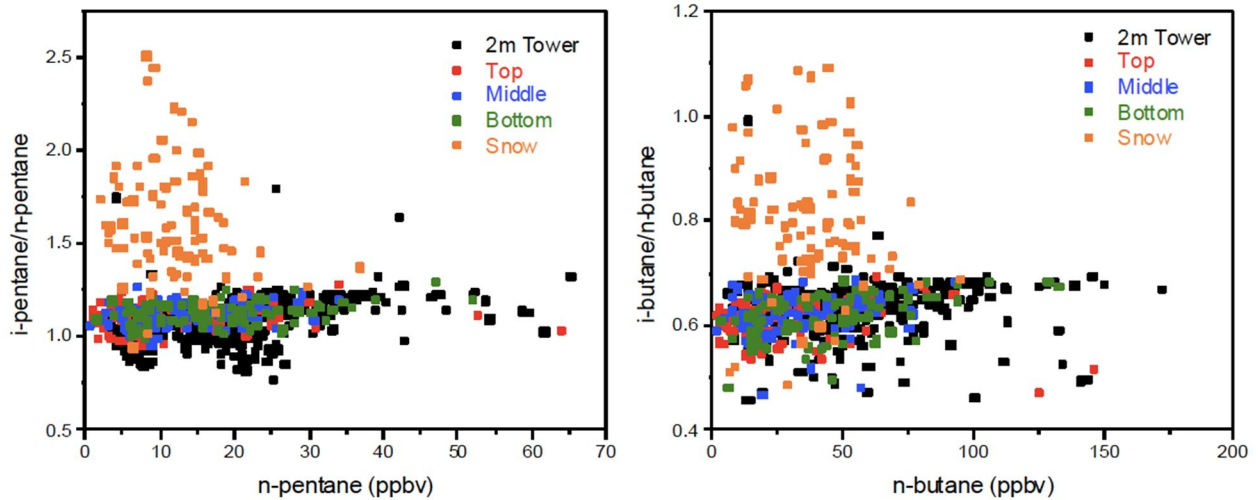


Figure 6-18. Plots of the iso-pentane:n-pentane ratio versus n-pentane and the iso-butane:n-butane ratio versus n-butane for all NMHC data divided by inlet height.

6.3.6 Meteorological Parameters

The vertical distribution of potential temperature as measured from the balloon soundings is shown in Figure 6-19. This graph illustrates the persistence of the temperature inversion with coldest temperatures and strongest inversions coinciding with the periods of strongest ozone production. The pressure record in Figure 6-20 nicely illustrates how the periods with lower ozone precursor concentrations and lower ozone buildup occurred during times when low pressure systems had moved into the region.

March 2014

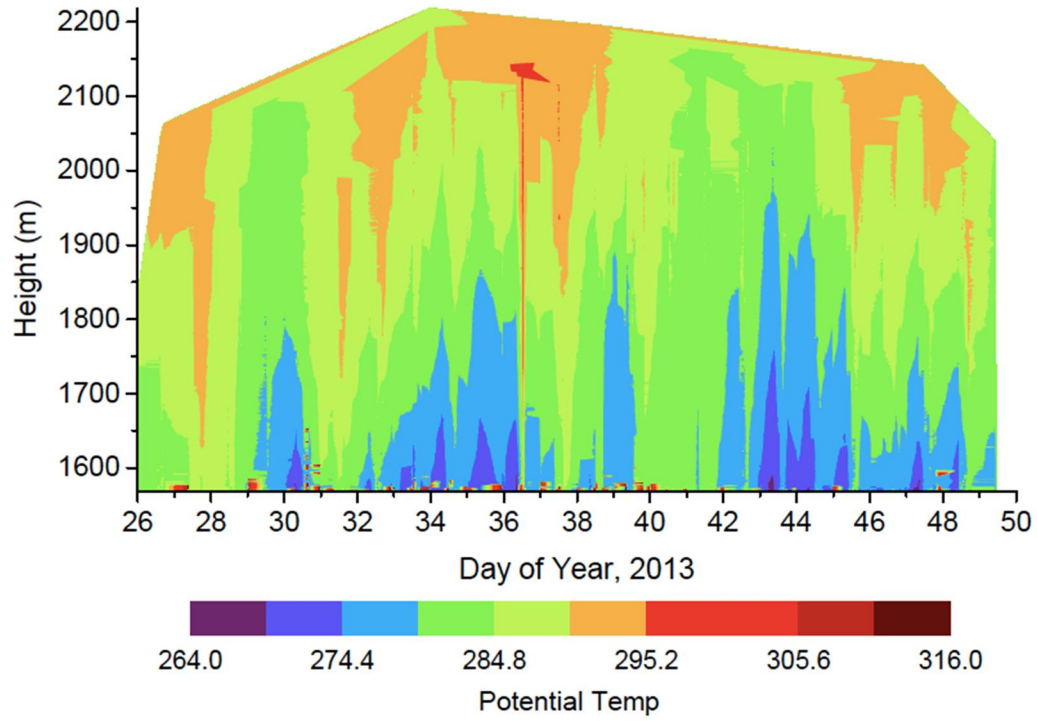


Figure 6-19. Potential temperature vertical distribution from the tether sonde data.

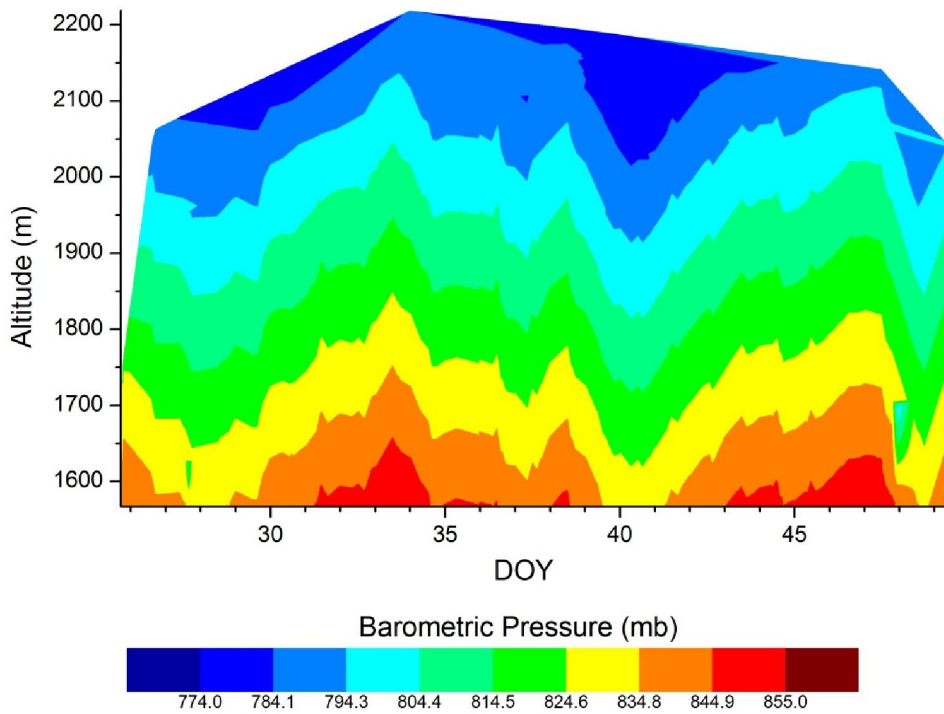


Figure 6-20. Pressure record from the tether sonde vertical balloon profiles.

6.4 References

- Albert, M. R., A. M. Grannas, J. Bottenheim, P. B. Shepson, and F. E. Perron (2002), Processes and properties of snow, Air transfer in the high Arctic with application to interstitial ozone at Alert, Canada, *Atmospheric Environment*, 36(15), 2779-2787.
- Ariya, P., B. Jobson, R. Sander, H. Niki, G. Harris, J. Hopper, and K. Anlauf (1998), Measurements of C2-C7 hydrocarbons during the Polar Sunrise Experiment 1994: Further evidence for halogen chemistry in the troposphere, *Journal of Geophysical Research*, 103(D11), 13169.
- Bocquet F., D. Helmig, and S.J. Otlans (2007), Ozone in interstitial air of the mid-latitude snowpack at Niwot Ridge, Colorado. Arctic, *Antarctic and Alpine Research* 39, 375-387.
- Boudries, H., and J. Bottenheim (2000), Cl and Br atom concentrations during a surface boundary layer ozone depletion event in the Canadian high Arctic, *Geophysical Research Letters*, 27(4), 517-520.
- Helmig, D., F. Bocquet, L. Cohen, and S. J. Oltmans (2007), Ozone uptake to the polar snowpack at Summit, Greenland, *Atmospheric Environment*, 41(24), 5061-5076.
- Jobson, B., H. Niki, Y. Yokouchi, J. Bottenheim, F. Hopper, and R. Leitch (1994), Measurements of C2-C6 hydrocarbons during the Polar Sunrise 1992 Experiment: Evidence for Cl atom and Br atom chemistry, *J. Geophys. Res.*, 99(D12), 25355 - 25368.
- Peterson, M., and R. Honrath (2001), Observations of rapid photochemical destruction of ozone in snowpack interstitial air, *Geophysical Research Letters*, 28(3), 511-514.
- Pszenny, A. A., E. V. Fischer, R. S. Russo, B. C. Sive, and R. K. Varner (2007), Estimates of Cl atom concentrations and hydrocarbon kinetic reactivity in surface air at Appledore Island, Maine (USA), during International Consortium for Atmospheric Research on Transport and Transformation/Chemistry of Halogens at the Isles of Shoals, *Journal of Geophysical Research: Atmospheres*, 112(D10).
- Rudolph, J., B. Ramacher, C. Plass-Dülmer, K. Ä. Müller, and R. Koppmann (1997), The indirect determination of chlorine atom concentration in the troposphere from changes in the patterns of non-methane hydrocarbons, *Tellus B*, 49(5), 592-601.
- Rudolph, J., B. Fu, A. Thompson, K. Anlauf, and J. Bottenheim (1999), Halogen atom concentrations in the Arctic troposphere derived from hydrocarbon measurements: Impact on the budget of formaldehyde, *Geophysical Research Letters*, 26(19), 2941-2944